

Discontinuum Modelling Approach for Stress Analysis at a Seismic Source: Case Study

Atsushi Sainoki¹ · Hani S. Mitri¹ · Mike Yao² · Damodara Chinnasane³

Received: 18 May 2016 / Accepted: 10 September 2016 / Published online: 19 September 2016
© Springer-Verlag Wien 2016

Abstract Rockbursts in underground mines can cause devastating damage to mine workings; hence, it is important to be able to assess the potential for their occurrence. The present study focuses on a large seismic event that took place at an underground base metal mine in Canada. The event took place in a dyke near the 100/900 orebodies on 3880 Level (1180 m below surface) of the Copper Cliff Mine in Sudbury, Canada. A 3D continuum stress analysis of the orebodies, i.e., 100 and 900, using an orebody-wide model encompassing the major geological structures and in situ stress heterogeneity in the mine shows low potential for rockburst at the seismic source location—a result which contradicts the fact that a large seismic event actually took place. A postulation is thus made that there had been highly stressed regions caused by geological disturbances at the source location before mining activities took place. In order to verify the postulation, a further study is undertaken with the discrete element modelling technique, whereby a cube-shaped model containing a fracture network is subjected to a stress state similar to that at the source location. A model parametrical study is conducted with respect to the distribution of the fracture (joint) network and its mechanical properties. The results reveal that when joints are densely distributed at the source location, the stress state becomes significantly burst prone. It is observed that the length, density, stiffness, and orientation of joints have a large influence on the stress state along the joints, while

the friction angle, cohesion, and tensile strength do not influence the stress state. A cube-shaped model is constructed with joint sets actually mapped at the mine and a stress analysis is performed. The results demonstrate the generation of highly stressed regions due to the interaction of the joints with the applied in situ stress fields, thus leading to burst-prone conditions. The present study numerically confirms that a preexisting fracture network found within a stiff rockmass could lead to burst-prone stress state at relatively moderate mining depths.

Keywords Rockburst · Discontinuum analysis · Fracture network · Stress analysis · Burst-prone condition

1 Introduction

In deep underground mines, mining activities, such as stoping and drift development, induce stress re-distribution and stress concentrations. Mining-induced stress change is the primary cause for rockburst occurrence in underground mines. Since the last century, rockbursts have been recognized as a serious hazard to safety, mine excavation and mining equipment (Blake and Hedley 2003; Ledwada et al. 2012; Ortlepp and Stacey 1994; Qiu et al. 2014). Although the magnitude of rockbursts varies depending on the source mechanism (Blake and Hedley 2003; Ortlepp and Stacey 1994), rockbursts with Richter magnitude >2.0 can occur when induced by the reactivation of preexisting faults or by violent propagation of shear rupture through an intact rockmass. According to Hedley (1992), a rockburst that has Nuttli magnitude of 3.0 can cause severe damage to a rockmass within approximately 20 m of its source location and cause the instability of underground openings, such as rock falls, in areas within a radius of 100 m. Rockburst

✉ Atsushi Sainoki
atsushi.sainoki@mail.mcgill.ca

¹ Department of Mining and Materials Engineering, McGill University, Montreal, Canada

² Vale Base Metals, Vale Canada Ltd, Sudbury, Canada

³ Vale Ontario Operations, Vale Canada Ltd, Sudbury, Canada

hazards are life-threatening (Heunis 1980) and could lead to a significant decrease in the driving rate of excavations (Ortlepp and Stacey 1994). A better understanding of rockburst phenomena is thus of paramount importance to ground control specialists as they strive to provide a safe working environment.

Significant efforts have been made in developing methods to evaluate rockburst potential in underground mines. The developed methods are generally classified into two types, namely stress and energy methods. The former examines the stress acting on the rockmass relative to its strength, while the latter focuses on energy stored in the rockmass. Martin and Kaiser (1999) indicated that brittle failure may take place when the ratio of the maximum tangential boundary stress to the laboratory unconfined compressive strength exceeds 0.4. Based on the study, Castro et al. (2012) proposed the brittle shear ratio (BSR), which is defined as the ratio of the difference between the maximum and minimum principal stresses to uniaxial compressive strength. It is shown that when the ratio is >0.7 , potential for rockbursts is significant. The studies mentioned above are stress-based methods. For the energy methods, Mitri et al. (1999) introduced the burst potential index (BPI), which takes into account the energy stored in rockmass before and after mining as well as the critical energy density representing the maximum energy per unit volume that rock can store. Alternatively, the stress–strain curve of a rock specimen is commonly used as an index for rockburst potential (Kidybinski 1981; Wawersik and Fairhurst 1970) because the curve represents the ratio of retained energy to dissipated energy during a loading test. Rockburst potential increases with the increasing proportion of retained energy.

As can be found from previous studies, a better understanding of the rock characteristics (stress–strain curve) and the in situ stress state is indispensable in the proper evaluation of rockburst potential. In fact, case studies reveal that the occurrence of a rockburst is strongly related to geological structures, which affect the local in situ stress distribution. McGarr et al. (1975) investigated mining-induced seismicity that took place in a deep underground gold mine in South Africa. The study showed that most seismic event source locations are situated away from the mining area, which is found to be inconsistent with the stress fields simulated based on measurements of ambient stress in the mine. The authors concluded that tectonic disturbances (shear and fracture zones) induce extremely high stress concentrations that cause intact rock to fail. Bewick et al. (2009) suggested that interactions between geological structures play a key role in the occurrence of seismic events and demonstrated with numerical simulations that geological structures with high stiffness attract high stress, compared to the surrounding regions. Likewise,

the stress state within heterogeneous rockmass was simulated by Shnorhokian et al. (2014) while applying calibrated stresses to the boundaries of an orebody-wide model. Sainoki and Mitri (2014) demonstrated that the heterogeneity of the rockmass within a shear zone significantly affects the evolution of fault-slip potential in the area. They showed that when the homogeneity of shear stiffness is assumed within the entire shear zone, fault-slip potential is not high enough to cause discontinuous planes within the shear zone to slip, whereas extremely high fault-slip potential is locally developed when variation in shear stiffness is taken into account. The variation in shear stiffness is assumed to be caused by either the difference in fracture density or strong interlocking fractures.

In light of previous studies, it is reasonable to conclude that the heterogeneity of the rockmass is strongly associated with the occurrence of rockbursts in underground mines; tectonically induced disturbed areas, stiff geological structures, and variation in the distribution of cracks and fractures within shear zones can be considered as the cause of the heterogeneity. It is therefore assumed that highly stressed regions locally occur in the rockmass with the aforementioned preexisting geological disturbances. In such regions, large seismic events can take place even if stress changes caused by mining activities are minimal. This mechanism is considered quite reasonable for rockbursts taking place away from a mining area (McGarr et al. 1975). It is to be noted, however, that the stress state within the geologically disturbed areas cannot be estimated with numerical simulations assuming the homogeneity of rockmass. The heterogeneity of rockmass needs to be taken into consideration (Sainoki and Mitri 2014).

The present study investigates the effect of preexisting joint network on the evolution of rockburst potential at the source location of a large seismic event recorded at the Copper Cliff mine in Sudbury, Canada. Using a 3D orebody-wide model, a stress analysis is performed with the finite difference method. The result shows that the in situ stress state at the seismic event source location is far below the maximum strength determined by a failure criterion and that BSR is quite small, indicating a low possibility of a large seismic event taking place. The result implies the limitations of the continuum modelling technique, although the stress analysis simulates highly stressed regions ascribed to stiff geological structures with the boundary traction method (Shnorhokian et al. 2014). Thus, the discrete element method is employed, whereby a fracture network is generated representing the jointed rockmass. A model parametrical study is undertaken with respect to the properties of the joint network, such as joint density, orientation, and mechanical properties. Based on the results, the effect of joint network on burst potential is analyzed. Finally, a model including joint sets actually observed at

the mine is constructed. It is then demonstrated that the stress state at the source location of the seismic event can become significantly higher due to the presence of joint network causing stress concentration.

2 Copper Cliff Mine

A case study is undertaken for the Copper Cliff mine in Sudbury, Canada. This section is dedicated to describing a 3D orebody-wide model representing the geological structures in the mine.

2.1 3D Orebody-Wide Model

The 3D orebody-wide shown in Fig. 1 encompasses major geological structures in the area of interest in the mine. The outer boundaries are situated at least 300 m away from the geological structures. The model domain is discretized into tetrahedral zones in order to perform a stress analysis with FLAC3D (Itasca 2009), which employs a finite difference method.

As shown in Fig. 1, the 3D orebody-wide model is 2352 m in height, 1930 m in length, and 1194 m in width. The x - and y -directions in the model correspond with east and north, respectively. The total numbers of zones and grid points in the model are 765,796 and 129,486, respectively. The model extends from 500 Level (152 m below the surface) to 8200 Level (2500 m below the surface), which is considered sufficiently large to analyze the

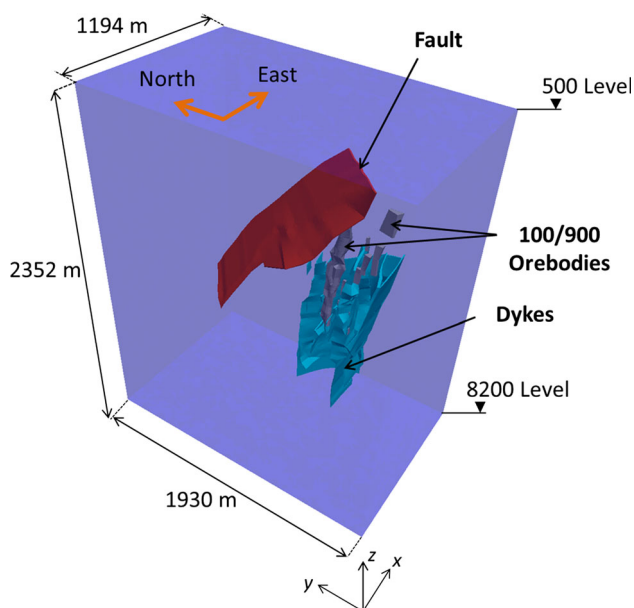


Fig. 1 Isometric view of 3D orebody-wide model including the 100/900 orebodies and the important geological structures at the Copper Cliff mine in Sudbury, Canada

stress state in the mine while taking into account the effect of the geological structures. Coarse meshes are generated near the model outer boundaries, and the meshes gradually become finer toward the geological structures inside the model.

2.2 Geological Structures in the Mine

The detailed geometries of the orebodies are shown in Fig. 2. The 100 and 900 orebodies are sub-parallel and in close proximity to each other. The 100 orebody typically consists of inclusions of massive-to-heavily disseminated sulfide mineralization, while the 900 orebody consists of mostly erratic sulfide stringers and lenses with some disseminated mineralization. The main host rock for the orebodies is predominantly massive quartz diorite, which is primarily comprised of amphibole, biotite, and chlorite. The fault dips at 45° to the north and consists of strongly sheared, black biotite schist and minor carbonate mud gouge within its boundaries. The width of the fault varies from 3.6 to 4.6 m, and it has created very blocky, semi-vertical joint systems up to 6 m on each side.

In the vicinity of the 100 and 900 orebodies, there are a number of discontinuous olivine and quartz diabase dykes that crosscut the orebodies and intersect a younger felsic intrusive rock. There is also a significant trap dyke that lies between the two orebodies. In situ observation of the rock joints was made for exposed dyke on 3710 Level situated above 3880 Level on which the large seismic event being examined in the present study had occurred. It was impossible to observe the joints on 3880 Level because the drifts are at present completely covered with shotcrete. Joints shown in Fig. 3 are examples measured during the

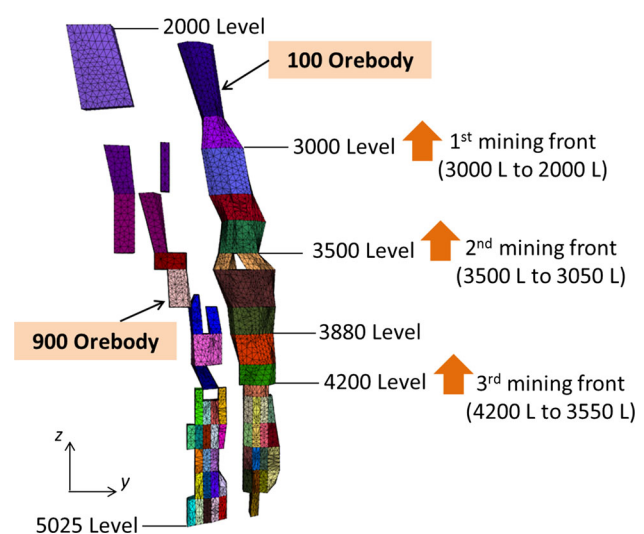


Fig. 2 100 and 900 orebodies extending from the 5025 Level to the 2000 Level and mining directions for first, second, and third mining fronts



Fig. 3 Example of joints observed on the surface of exposed dyke on 3710 Level

Table 1 Joint sets observed on the surface of dyke on 3710 Level

Joint set	Mean dip angle (°)	Mean dip direction (°)	Spacing (m)
1	80	68	0.15
2	25	118	0.15
3	79	272	0.05
4	90	127	0.1

observation. As can be seen in the figure, there are prominent joints in the dyke.

Table 1 lists the observed joint sets. It is to be noted that the number of joints that was observed on 3710 Level is limited due to the shotcrete covering the drifts. Therefore, it is unclear whether the observed joint sets are present in the entire dyke. However, it is evident that the dyke locally has those joint sets with narrow spacing as shown in the table.

The modelled geological structures extend well below and above the 3880 Level where the large seismic event took place. Also, the orebodies between 3550 and 5025 Levels are being examined. In order to consider the effect of past mining activities, the constructed orebody-wide model encompasses the 100 and 900 orebodies between 2000 and 3550 Levels as well as the geological structures between and around the levels, but the geological structures on far deeper and shallower levels are not modelled as their influence on the stress state in the areas of interest is negligible.

2.3 Analysis of the Seismic Event

The present study examines the large seismic event that took place on 3880 Level. The seismic monitoring system in this mine consists of 9 triaxial and 36 uniaxial

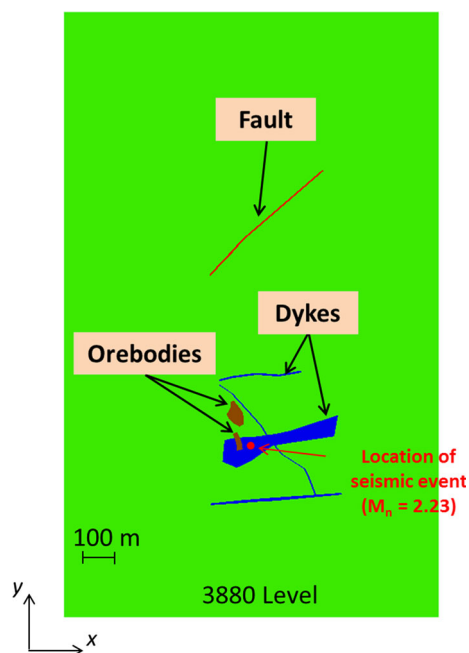


Fig. 4 Plan view of 3880 Level showing geological structures and the source location of a large seismic event that took place in the past

accelerometers. Possible error ranges from 3 m (10 feet) to 15 m (50 feet). The source location of the seismic event is shown in Fig. 4. As can be seen in the figure, the seismic source is located inside the dyke and near the orebodies. Unlike seismic events taking place away from active mining areas (Bewick et al. 2009), the seismic source location is reasonable since the dyke is assumed to carry higher stress compared to the surrounding rockmass due to its high stiffness. In addition, it is assumed that the source location is in the area affected by stress re-distribution resulting from the stope extraction. As shown in Fig. 2, the mining activity first started on 3000 Level in accordance with the mining sequence as per the sublevel stopping

method with delayed backfill. The blocks from the 4200 Level to the 3550 Level (3rd mining front) and the 3500 Level to the 3050 Level (2nd mining front) were mined out simultaneously until the end of 2008. The seismic event took place when mining activities reached the 3880 Level.

The moment magnitude of the seismic event estimated from the waveforms recorded by a strong ground motion sensor is M_w 2.23. Based on the chart describing the range of magnitude for each type of rockburst proposed by Ortlepp and Stacey (1994), it is postulated that the seismic event was induced by shear rupture through an intact rock. The fact that no preexisting faults are present around the source location eliminates the possibility that the seismic event was caused by the reactivation of a fault. In addition, as the seismic event took place away from the mined stopes, face burst or strain burst is excluded as a cause of the seismic event.

3 Stress Analysis with the Copper Cliff Orebody-Wide Model

In order to examine the stress state at the seismic source location, a stress analysis is performed. The present study calibrates the premining stress state in the numerical model with the boundary traction method (Shnorhokian et al. 2014).

3.1 Material Properties of the Rockmass in the Copper Cliff Mine

Rock samples were collected from the geological structures, and uniaxial compressive tests were performed to estimate the mechanical properties of the rock specimens. Average values of the experimental results, namely modulus of elasticity for intact rock, E_{intact} , Poisson's ratio, ν , unit weight, γ , and uniaxial compressive strength, σ_c , are listed in Table 2. It is noticed from the table that E_{intact} and σ_c for the dyke are comparatively high, implying that the dyke can store large elastic energy and become burst prone.

The rockmass rating system (RMR) developed by Bieniawski (1976) is used for the 100 and 900 orebodies. The results show that RMR for the 100 orebody varies

from 65 to 75, while RMR for the 900 orebody ranges from 60 to 65. Considering the results, RMR of 65 is assumed. The same RMR is assumed for the host rock due to lack of information. Using the RMRs, modulus of elasticity for the rockmasses are calculated with the equation proposed by Mitri et al. (1994). For the dyke, E_{rockmass} is not estimated, considering the fact that rock with high stiffness attracts higher stress. It means that assuming RMR = 100 is the most conservative when estimating the potential for seismic events. For the fault, likewise, E_{intact} is used because the estimated E_{intact} is considerably low, compared to those for the other rocks. Hence, the scale effect is not taken into account. The unit weight of the dyke and the fault are assumed to be the same as that of the host rock.

3.2 In Situ Stress State

The calibration of premining stress state is conducted while applying stresses to the model external boundaries, based on the stress–depth relationships used at Copper Cliff mine. The stress–depth relationships are almost identical to those proposed by Herget (1987) and Diederichs (1999) for the Canadian Shield. Comparison of the stress–depth relationships is made in Fig. 5. As can be seen, the calculated stress–depth relationships give almost the same results as those adopted in the present study, which are expressed as follows:

$$\sigma_{H_{\max}}^o = 0.0407 \times D + 10.35 \quad (1)$$

$$\sigma_{H_{\min}}^o = 0.0326 \times D + 8.69 \quad (2)$$

$$\sigma_v^o = 0.029 \times D \quad (3)$$

where D represents the mining depth in meters. The calibration of premining stress in the Copper Cliff mine is performed on the basis of stresses calculated from Eqs. (1) to (3). Note that the trend of the maximum horizontal stress coincides with the x -direction in Fig. 1.

3.3 Calibration of Premining Stress State in the Copper Cliff Orebody-Wide Model

The boundary traction method simulates high stress concentrations caused by heterogeneous geological conditions

Table 2 Rockmass mechanical properties obtained from laboratory tests

	E_{intact} (GPa)	E_{rockmass} (GPa)	ν	γ (kN/m ³)	σ_c (MPa)
Host rock	52	37.8	0.24	28.5	94
Orebody	38	27.6	0.28	36.3	78
Dyke	60	N/A	0.22	28.5	220
Fault	0.4	N/A	0.25	28.5	62

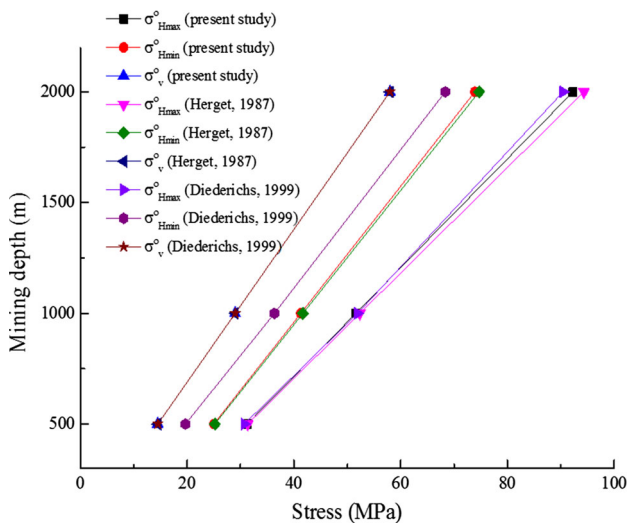


Fig. 5 Comparison of calculated pre-mining stresses based on stress-depth relationships with those adopted in the present study

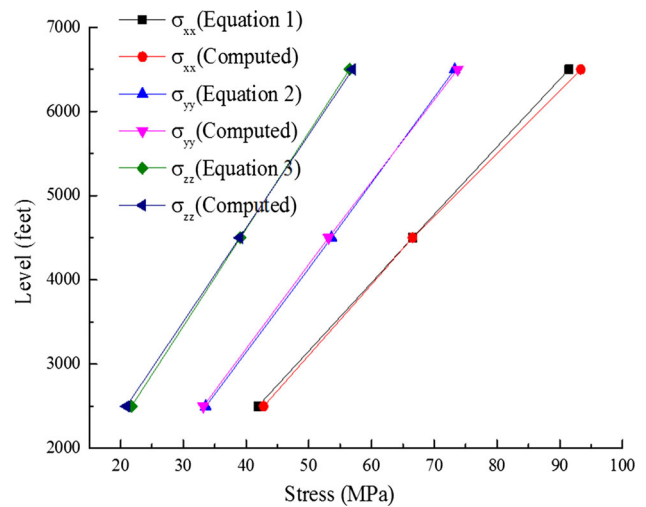


Fig. 7 In situ stress state at three observation points after calibrating the stresses applied to the model boundaries

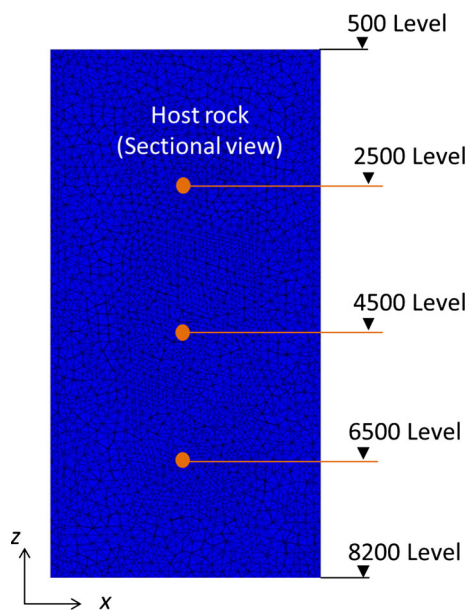


Fig. 6 Sectional view showing observation points for in situ stress calibration

at the premining stress state (Bewick et al. 2009; Shnorhokian et al. 2014). The calibration of premining stress is conducted based on the stress states at the observation points shown in Fig. 6. The observation points are located in the host rock that is away from the geological structures because the employed stress–depth relationships represent a far-field stress field.

Figure 7 shows the stress states at the observation points after calibrating the stresses applied to the model boundaries. As shown in the figure, stresses calculated from the equations agree reasonably well with those at the observation points.

3.4 Stress Analysis at the Seismic Source Location

Stopes in the orebodies are extracted in accordance with the mining sequence, based on the calibrated premining stress state. When the mining sequence reaches 3880 Level, the stress state is examined at the source location in Fig. 4 and compared with that at the premining stage.

Figure 8 shows differential stress (σ_{dif}) defined as the difference between σ_1 and σ_3 . As shown in Fig. 8a, the differential stress in the dyke is obviously higher than that in the host rock at the premining stage. It confirms that high-stress state within stiff rockmass is successfully simulated with the boundary traction method. Figure 8b shows that the stope extraction increases differential stress at the source location, suggesting that the mining-induced stress change triggered the seismic event. Table 3 lists the minimum and maximum principal stresses at the source locations before and after the mining activities as well as the differential stress and brittle shear ratio (BSR). BSR is expressed with the following equation:

$$BSR = \frac{\sigma_1 - \sigma_2}{\sigma_3} \tag{4}$$

In the table, σ_c is the uniaxial compressive strength of the dyke. It can be seen that the increase in the differential stress at the source location is attributed to a slight increase in the maximum principal stress and a large decrease in the minimum principal stress. According to the increase in differential stress, BSR increases from 0.17 to 0.22 at the source location.

The result is considered quite reasonable because the increase in the maximum principal stress and the decrease in the minimum principal stress are directly related to the rise in the potential for rockburst caused by the shear

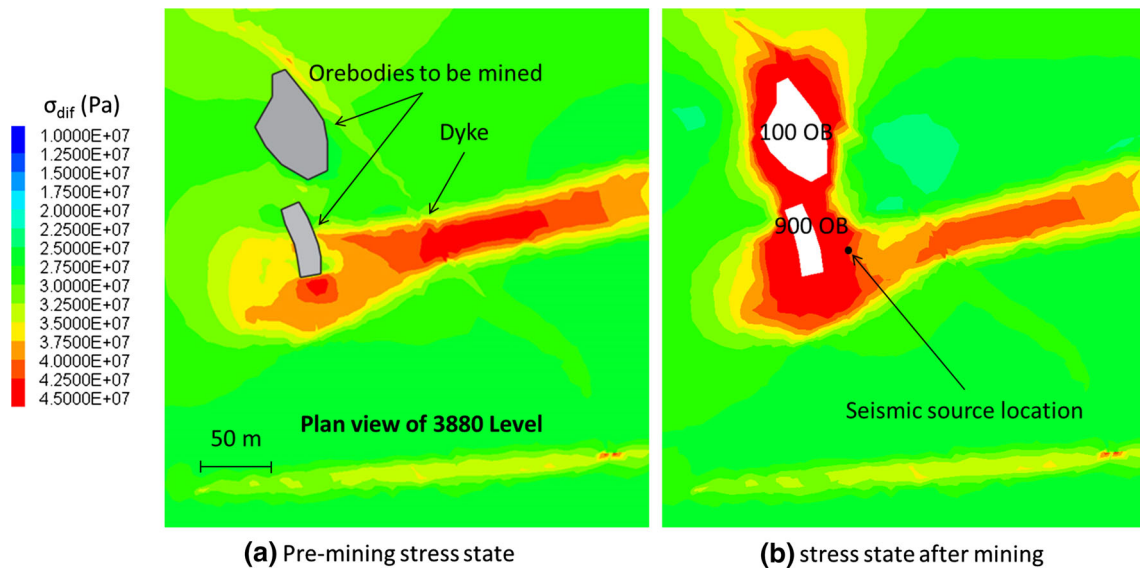


Fig. 8 Plan view of 3880 Level showing differential stress before and after mining activities

Table 3 Stress state at the seismic source location

	σ_1 (MPa)	σ_3 (MPa)	σ_{dif} (MPa)	Brittle shear ratio (BSR) (σ_{dif}/σ_c)
Before mining	75.0	37.1	37.9	0.17
After mining	77.9	29.3	48.6	0.22

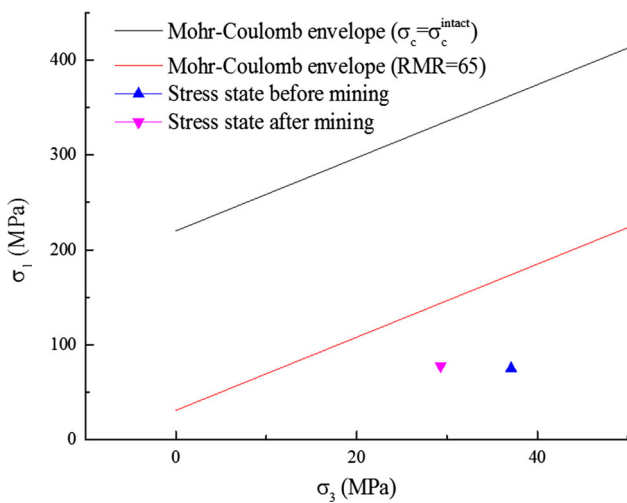


Fig. 9 Comparison of stress states at the seismic source location with the Mohr-Coulomb failure envelope

failure of rockmass. However, further discussion is required with respect to the magnitude of the differential stress. As shown in Table 3, the brittle shear ratio after the stope extraction is 0.22, which is far below the criterion representing high potential for rockburst (Castro et al. 2012). According to Castro et al. (2012), the risk of strain burst is considered zero when BSR is <0.35, although, as discussed in the previous section, the seismic event is more

significant than one caused by strain burst. Assuming that the rockburst was caused by the instantaneous shear failure of rockmass, plotting the stress state at the source location along with a failure envelope gives an insight into the potential for rockburst. In Fig. 9, two Mohr–Coulomb failure envelopes are delineated. The upper failure envelope represented by the black line assumes that the uniaxial compressive strength of dyke is the same as that of the intact rock. For the failure envelope represented by the red line, the uniaxial compressive strength is decreased, assuming that RMR of dyke is the same as that of the orebodies. The friction angle of the dyke is assumed to be 36°, based on the case study for the mine located in the same region (Sainoki and Mitri 2014). It is found from Fig. 9 that the stress state is situated far below both the Mohr–Coulomb failure envelopes. The calculated BSR in Table 3 and the stress state plotted in Fig. 9 explicitly suggest that it is highly improbable that shear failure takes place at the location.

By performing a back analysis, a friction angle at which the stress state reaches the Mohr–Coulomb failure envelope is calculated. The equation for the back analysis is as follows:

$$\phi = \sin^{-1} \left(\frac{\sigma_1 - \sigma_3}{\sigma_1 + \sigma_3} \right) \tag{5}$$

By substituting the maximum and minimum principal stresses after the stope extraction shown in Table 3 into Eq. (5), the friction angle is calculated to be 26° . It means that shear failure can occur when the friction angle and the cohesive strength of dyke are 26° and zero, respectively. Hoek and Brown (1997) suggested a friction angle of 46° and cohesive strength of 13 MPa as the mechanical properties of a very good quality hard rockmass, and a friction angle of 33° and cohesive strength of 3.5 MPa are suggested for an average quality hard rockmass. Obviously, the shear strength of the dyke estimated above is extremely low. If there are faults containing a prominent slip surface with a low basic friction angle (Alber and Fritschen 2011), seismic events can occur at the source location. However, according to the geological surveys conducted at the mine, no faults are present at the source location.

In light of these results, it is postulated that there had been highly stressed regions caused by localized geological disturbances, such as preexisting fractures and/or joints, around the source location before the mining activity began and that the seismic event was triggered by the mining-induced stress change. Although the heterogeneous stress condition caused by the stiff rockmass can be simulated with the boundary traction method, the stress analysis results imply the limitation of the conventional continuum analysis.

4 Stress Analysis at the Seismic Source Location with the Discrete Element Method

The established hypothesis is tested with a numerical model including a fracture network. Figure 10 illustrates the idea behind the postulation, that is, the fracture zones

generated under the stress state in the past are re-stressed under the present stress state and/or mining-induced stress while producing highly stressed areas. Hence, the boundary traction method is employed in order to simulate stress concentrations caused by the preexisting fracture network subjected to stress regime different from that under which it occurred.

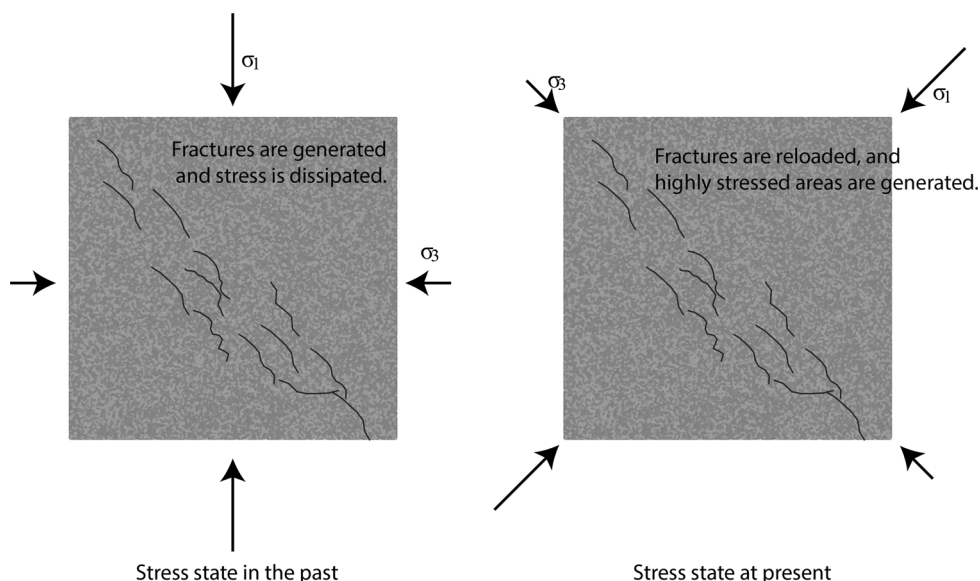
4.1 Model Parametrical Study

4.1.1 Construction of a Numerical Model with Fracture Network

The numerical model including a fracture network is constructed by means of 3DEC (Itasca 2014), which is a three-dimensional numerical program employing the distinct element method for discontinuum modelling. Figure 11 shows a base model for the model parametrical study. The base model is cube-shaped, and its edge length is 5 m. As the primary purpose of this numerical modelling approach is to simulate high-stress regimes at the seismic source location, the model size is deemed sufficiently large.

Discontinuities representing fractures and joints are incorporated into the numerical model after dividing the model into small cubes with vertical and horizontal planes. The cutting is carried out in order to simulate prescribed lengths of discontinuities. Otherwise, simulated discontinuities cut through the entire model. Therefore, it is to be noted that the horizontal and vertical lines in Fig. 11 do not represent discontinuities. Figure 12 depicts three sets of joints generated in the base model. As shown in the figure, the dip angle and the dip direction of joints vary, even if they belong to the same joint set. This is due to a

Fig. 10 Schematic illustration showing the generation process of highly stressed area in localized geologically disturbed zones



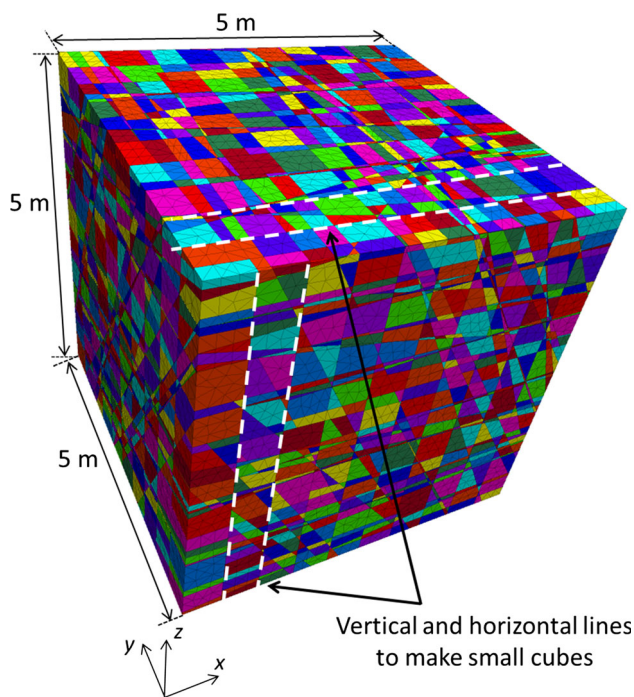


Fig. 11 Isometric view of a base model representing fractured and jointed rockmass

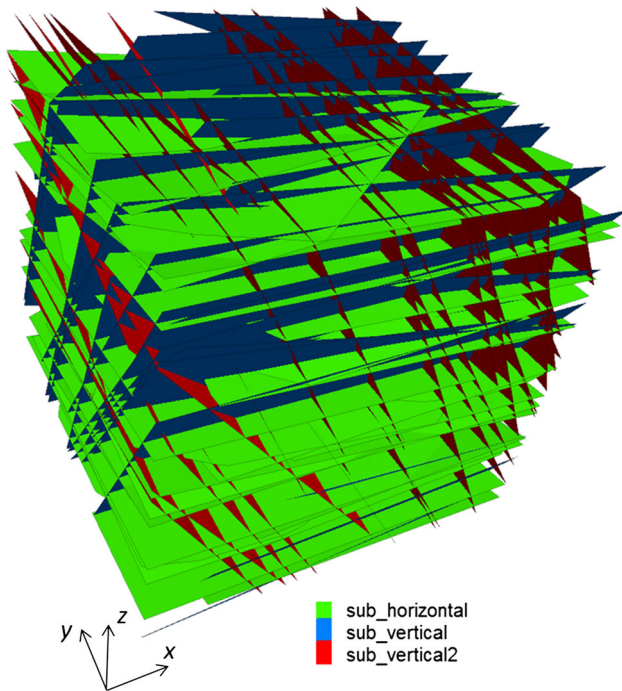


Fig. 12 Simulated discontinuous planes (joint sets) in the base discrete element model

probability function in 3DEC. Table 4 lists the properties used to generate the joint sets.

In the table, the dip direction is measured positive clockwise in the horizontal plane from the y-axis in

Fig. 11, and κ is the Fisher constant in the Fisher distribution (Fisher 1996), which is used to statistically determine the dip angle and dip direction of the joints and expressed as follows:

$$f(\theta) = \frac{\kappa \sin \theta \exp(\kappa \cos \theta)}{\exp(\kappa) - \exp(-\kappa)} \quad (6)$$

where θ is the angular deviation from a mean value. With regard to the fracture size distribution, it is generally accepted that fractures in nature follow a power law distribution (Hooker et al. 2014; Ortega et al. 2010). The constants, α and a , in the table are used in the power law equation expressed as:

$$n(l) = \alpha \cdot l^{-a} \quad (7)$$

where n is the number of fractures with the length of l per unit of volume; α is related to fracture density; a defines the ratio between fracture sizes, i.e., the proportion of small fractures to large fractures increases as a increases. For the base model, the minimum length of fractures (l_{\min}) is set to 5 m, which is equal to the edge length of the numerical model. Thus, a does not play an important role in determining the size distribution of fractures simulated for the base model.

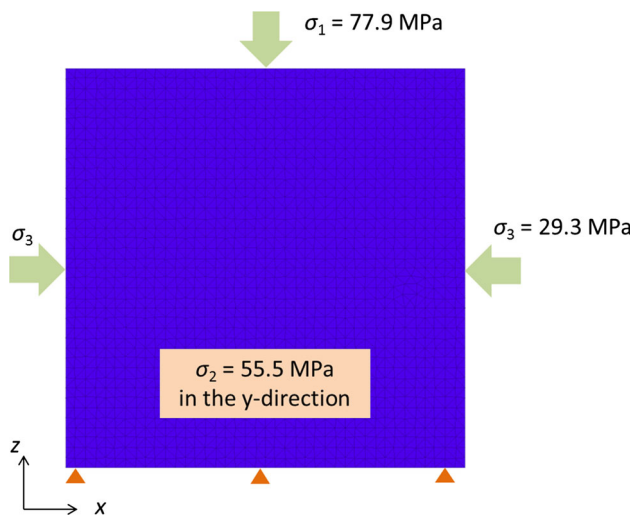
4.1.2 Preliminary Analysis to Determine an Appropriate Mesh Size

After incorporating prescribed discontinuities into the model, the model is discretized with deformable tetrahedral meshes. As the mesh size is assumed to have a large influence on numerical analysis results, a preliminary analysis is performed to determine an appropriate mesh size. The stresses applied to the model boundaries (Fig. 13) are obtained from the seismic source location. Note that the coordinate system in Fig. 11 does not coincide with that in Fig. 1. After the stress state in the model reaches equilibrium, BSR is calculated for each zone.

Regarding the mechanical properties of the rockmass in the model, the same properties as those for dyke are applied. Table 5 lists the mechanical properties of discontinuities produced in the base model. According to Barton and Choubey (1977), the friction angle of a typical rock joint falls into a range from 21° to 38°. The friction angle, 30°, in the table is an intermediate value in the range. Previous studies (Barton 1973, 2013) suggest that a rock joint has no cohesive strength when there is no infilling material on its surface. The shear strength characteristic of a rock joint is simulated adequately with the nonlinear model (Barton and Choubey 1977), which does not have a variable representing cohesion; instead, joint surface roughness is taken into account. However, when the nonlinear behavior of the shear strength is

Table 4 Properties used to generate fracture network for the base model

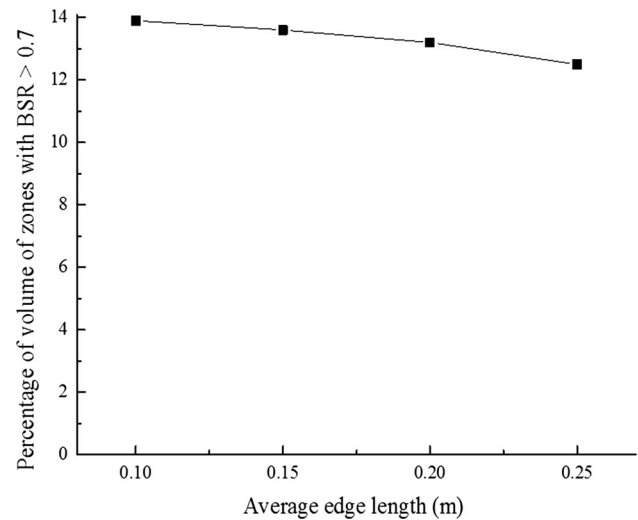
	Mean value of dip angle (°)	Mean value of dip direction (°)	κ	α	a	l_{\min} (m)
Sub horizontal	10	0	200	4	4	5
Sub-vertical	60	0	200	4	4	5
Sub-vertical 2	60	90	200	4	4	5

**Fig. 13** Stresses applied to the boundaries of the discrete element model**Table 5** Mechanical properties of fractures for the base model

Friction angle (°)	Cohesion (MPa)	Tensile strength	Normal stiffness (GPa/m)	Shear stiffness (GPa/m)
30	0.1	0	1	1

approximated with the classical Mohr–Coulomb criterion, cohesion appears as an intercept and thus needs to be taken into consideration, although the value is low. For the base model, the cohesion of discontinuities is assumed to be 0.1 MPa. With respect to the stiffness of a rock joint, its estimation is not straightforward as described by Bandis et al. (1983). In fact, the stiffness of a rock joint is dependent upon not only the physical properties of its surface, such as joint aperture and joint wall compressive strength, but also normal and shear displacements that the joint experienced in the past. Hence, for the base model, the value is simply assumed to be 1 GPa/m for the normal and shear stiffness. Effects of the mechanical properties of a discontinuity are examined in the model parametrical study.

The results obtained from the preliminary analysis are summarized in Fig. 14, which plots the percentage of volume of zones with $BSR > 0.7$ to the total volume

**Fig. 14** Results of preliminary analysis to determine an appropriate edge length of tetrahedral meshes generated in the model

(125 m³) with respect to the mesh sizes examined. As shown in the figure, it is evident that the fracture network changes the stress state at the source location to being burst-prone, i.e., BSR significantly increases from 0.22 shown in Table 3. A detailed discussion is given in a later section. With respect to the effect of the mesh size, it is found from the results that although the percentage increases with the decreasing average edge length, there are no noticeable differences among the results. Therefore, an average edge length of 0.15 m is adopted.

4.1.3 Properties to be Analyzed for a Model Parametrical Study

The mechanical and physical characteristics of fractures and/or joints are expected to exert a large influence on the stress state produced within the geologically disturbed zones. Hence, a model parametrical study is undertaken while changing the properties of simulated discontinuities. Specifically, effects of the following properties are examined, namely length, density, dip angle, dip direction, stiffness, friction angle, cohesive strength, tensile strength, and the constant, κ , in the Fisher distribution. The effect of the constant, a , in Eq. (7) is not examined as its effect can be investigated and discussed in examining the fracture length.

4.1.4 Analysis Procedure and Conditions

Analysis procedure and conditions for the model parametrical study are the same as those for the preliminary analysis. The use of the elastic constitutive model is intended to estimate the maximum potential for rockburst that could occur under the stress regime. In reality, when compressive or tensile stress of rock reaches its peak strength, failure occurs while causing reduction in the strength when the rock exhibits strain-softening behavior (Diederichs et al. 2004; Pola et al. 2014). This means that energy stored in the rock is dissipated due to the generation and coalescence of cracks. In addition to that, the propagation of the preexisting fractures can occur, depending on the ambient stress state (Hoek and Bieniawski 1965; Hoek and Martin 2014). These phenomena strongly affect the in situ stress state. It is to be noted, however, that rock failure and the propagation of preexisting fractures can be the causes for seismic events. The primary purpose of this study is to examine fracture network-induced high stress concentrations that lead to rockbursts, that is, high stress concentrations before rockbursts take place. Thus, simulating rock failure and the initiation of cracks as well as the propagation of fractures is not the scope of the present study.

4.1.5 Results and Discussion for the Model Parametrical Study

Figure 15 shows the effect of discontinuities on the maximum compressive stress. As can be seen in Fig. 15a, when there are no discontinuities in the model, the stress state is perfectly homogeneous, and the maximum compressive stress in the model coincides with the stress applied to the top boundary, which corresponds to the maximum stress at the seismic source location. The increase in the maximum compressive stress due to the fracture network is explicitly shown in Fig. 15b. The homogeneous stress state in Fig. 15a is changed to heterogeneous, complex stress fields with the presence of discontinuities. The stress state indicates that the discontinuities prevent the stress applied to the outer boundaries from being transferred inwards, resulting in highly stressed regions along the discontinuities near the outer boundaries, while the maximum compressive stress inside the model becomes lower.

The stress state in the base model shown in Fig. 15b is further analyzed with BSR. BSR is mainly used to assess the potential for strain burst; nevertheless, it can be used as one of indices to evaluate the potential for seismic events caused by the shear failure of rockmass because BSR is a function of differential stress ($\sigma_1 - \sigma_3$), which corresponds to twice the magnitude of the maximum shear stress. Thus, the increase in BSR has the same meaning as the increase in shear stress. Figure 16 clearly shows the increase in BSR due to the presence of discontinuities. In the case of the

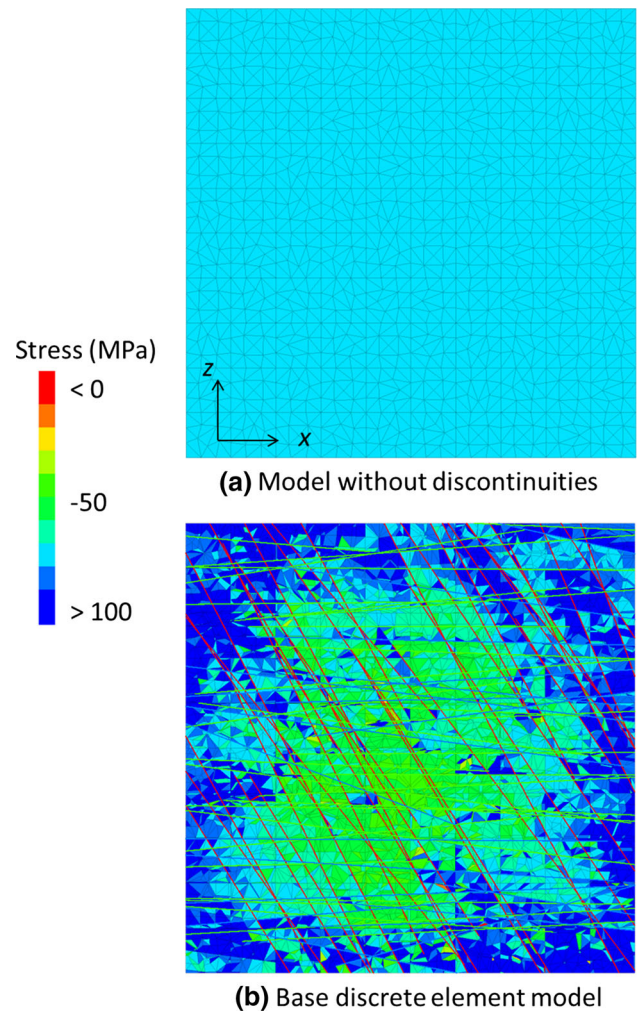


Fig. 15 Examples of maximum compressive stress in sectional views at $y = 2.4$ m

model without discontinuities, BSR is 0.22 throughout the model, while more than 13 % of the total volume (125 m^3) has $\text{BSR} > 0.7$ for the base discrete element model. $\text{BSR} > 0.7$ indicates that the potential for strain bursts is major (Castro et al. 2012). In total, more than 40 % of the total volume has BSR greater than that in the homogeneous model without discontinuities. Based on these results, it is reasonable to conceive that violent shear failure was caused by the combination of the stress concentrations due to preexisting discontinuities and the stress change resulting from the mining activities. The postulation established in the previous section is numerically verified.

Figure 17 shows the results of the model parametrical study with respect to model input parameters pertaining to fracture size distribution and its position. It is found from Fig. 17a that fracture density has a large influence on the stress state in the model. Note that the fracture density denotes the area of fractures per unit volume. When the fracture density is $4 \text{ m}^2/\text{m}^3$, the percentage is 13.6 %. The

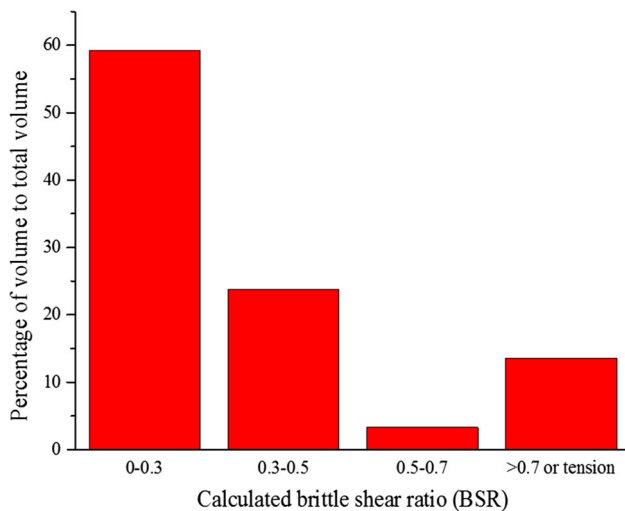


Fig. 16 Brittle shear ratio calculated for zones in the base discrete element model

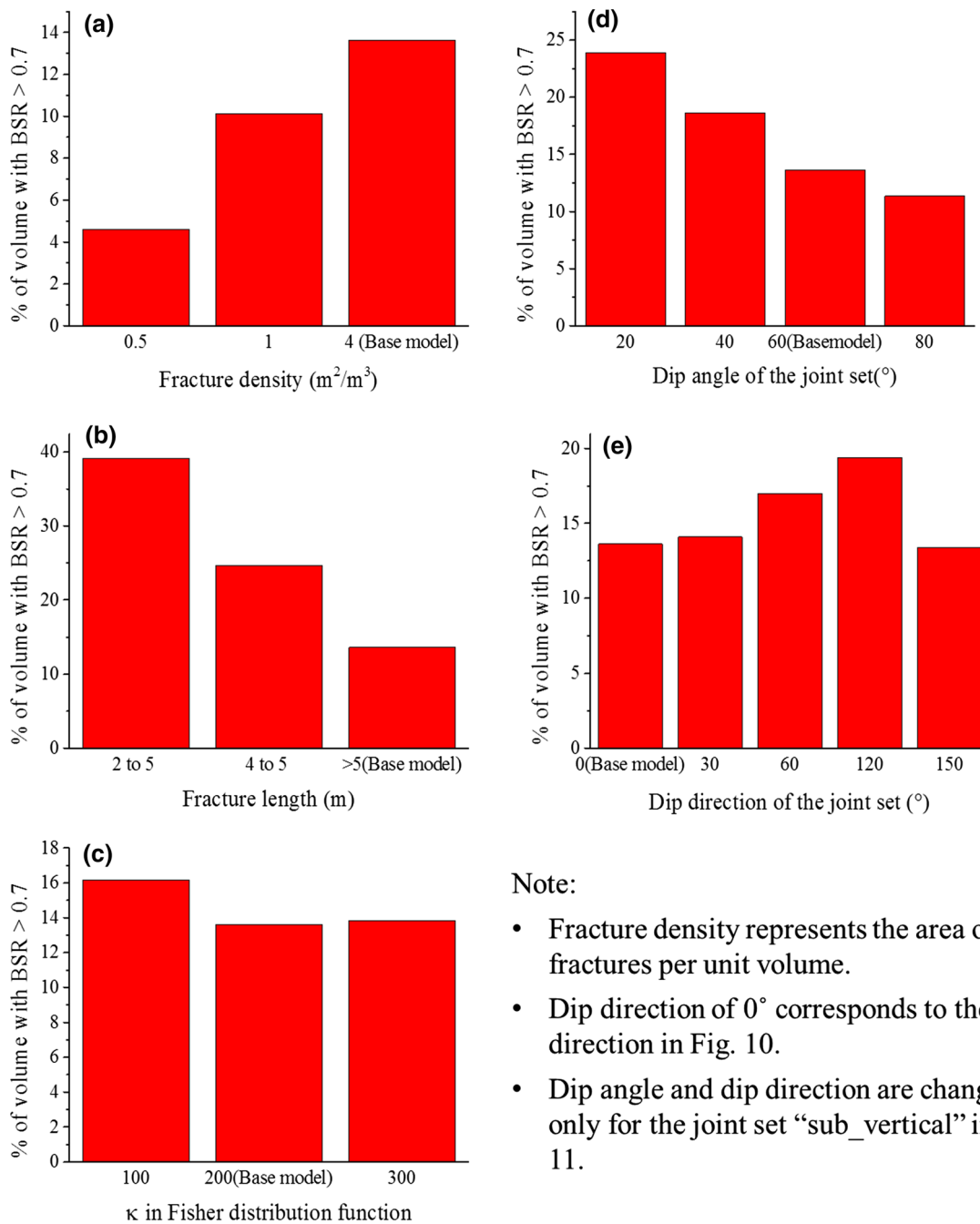
value decreases with the decreasing fracture density. When the fracture density decreases to $0.5 \text{ m}^2/\text{m}^3$, the percentage is no more than 4.6 %. The relation between fracture density and BSR is quite reasonable because more discontinuities interact with the stress field with the increasing fracture density. Figure 17b reveals that as fracture length decreases, the percentage of volume of zones with $\text{BSR} > 0.7$ significantly increases. When the maximum and minimum fracture lengths are set to 5 and 2 m, respectively, the percentage increases to 39 %. Figure 15b gives a plausible explanation about the relation between fracture length and stress state in the model. In the case of the base model, the minimum length of the discontinuities is 5 m, meaning that the discontinuities cut through the entire model. Thus, stress concentrations take place along the discontinuities situated near the external boundaries, as shown in the figure. When fracture length is set to <5 m, the stress applied to the model boundaries is transferred more inwards while generating complex stress field due to interactions with fractures inside the model. The parameter, a , in Eq. (7) is related to the ratio between fracture sizes; small fractures increases when the parameter increases. Hence, the effect of the parameter on the stress state in the model can be assumed based on the results in Fig. 17b. Figure 17c shows the effect of κ in the Fisher distribution function. As the constant decreases, simulated fractures become more heterogeneous while intersecting with each other. As expected from the characteristic, when the Fisher constant decreases, the volume of zones with $\text{BSR} > 0.7$ increases, although the increase is not significant. However, there seems to be no noticeable difference between models with $\kappa = 200$ and 300 , which would be attributed to the randomness of the discontinuity generation process. It means that when the model with $\kappa = 300$ was

constructed, the discontinuities were arranged in such a way that more stress concentrations take place. Consequently, the effect of κ is assumed to be cancelled out. The parametrical study with respect to the Fisher constant suggests that its effect on the stress field in the model is insignificant.

Figure 17d shows the effect of dip angle on the stress state in the model. It appears that the volume of zones with $\text{BSR} > 0.7$ increases with the decreasing dip angle of the joint set “sub-vertical” in Fig. 12. The relation is explained in terms of the trend of the maximum stress. As shown in Fig. 13, the maximum stress is applied to the model from its top boundary. It means that when the dip angle of the joint set is small, directions of normal vectors of the discontinuity planes is aligned with the orientation of the maximum stress, that is, the propagation of the stress from the boundary to the inward is interfered with the discontinuity planes while generating highly stressed regions as indicated in Fig. 15b. With regard to the effect of dip direction, the volume of zones with $\text{BSR} > 0.7$ increases when the dip direction ranges from 90° to 120° . The relation of dip direction with the increase in BSR is obscure, and its influence on the stress state is lesser, compared to dip angle. This is because the major factor that causes the stress concentration is the interaction of the maximum stress applied to the top boundary with the discontinuity planes, which does not significantly change when the dip direction is varied. Hence, it should be noted that when stress field is different from that simulated in the present study, the influence of the dip direction can be more significant than that of the dip angle.

Figure 18 shows results of the parametrical study with respect to the properties pertaining to the mechanical behavior of the discontinuities. The effect of stiffness of the discontinuities is shown in Fig. 18a. As can be seen in the figure, the stiffness significantly affects the stress state. As the stiffness increases, the volume of zones with $\text{BSR} > 0.7$ decreases, and vice versa. The relationship is due to the fact that a degree of heterogeneity in the model essentially attenuates with the increasing joint stiffness. When the stiffness is small, large displacements take place along the discontinuities, affecting stress fields of the surrounding zones.

Figure 18b–d shows effects of friction angle, cohesive strength, and tensile strength. It is found from the figures that the effects are negligible. This is because a slip along the discontinuities caused by excess shear stress theoretically never takes place under the current stress state as shown in Fig. 9. In the present study, the friction angle is changed from 30° to 40° , which falls into the reasonable range as the friction angle of dyke (Sainoki and Mitrì 2014). As calculated in the previous section, a friction angle of $<26^\circ$ is required in order for the discontinuities to



Note:

- Fracture density represents the area of fractures per unit volume.
- Dip direction of 0° corresponds to the y-direction in Fig. 10.
- Dip angle and dip direction are changed only for the joint set “sub_vertical” in Fig. 11.

Fig. 17 Effects of properties determining fracture size distribution and position on the stress state in the model

slip. If an extremely low friction angle is applied, it is conjectured that shear displacements take place along the discontinuities and the stress state undergoes a change.

4.1.6 Summary of the Model Parametrical Study

Summarized results of the model parametrical shown in Table 6 imply that the properties of a fracture network can be used as indices to assess the potential for rockburst in geologically disturbed regions. For instance, when there

are relatively short and dense fractures within a stiff rockmass, the potential for rockbursts would significantly increase. As can be seen in the table, the effects of friction angle, cohesion, and tensile strength on the potential for rockbursts are not evaluated, as the effect is negligible under the applied in situ stress state and can be assumed to become more significant if the in situ stress state is changed. It is suggested that further study be undertaken in the future in order to establish a new index that combines the effect of preexisting fracture network on in situ stress fields

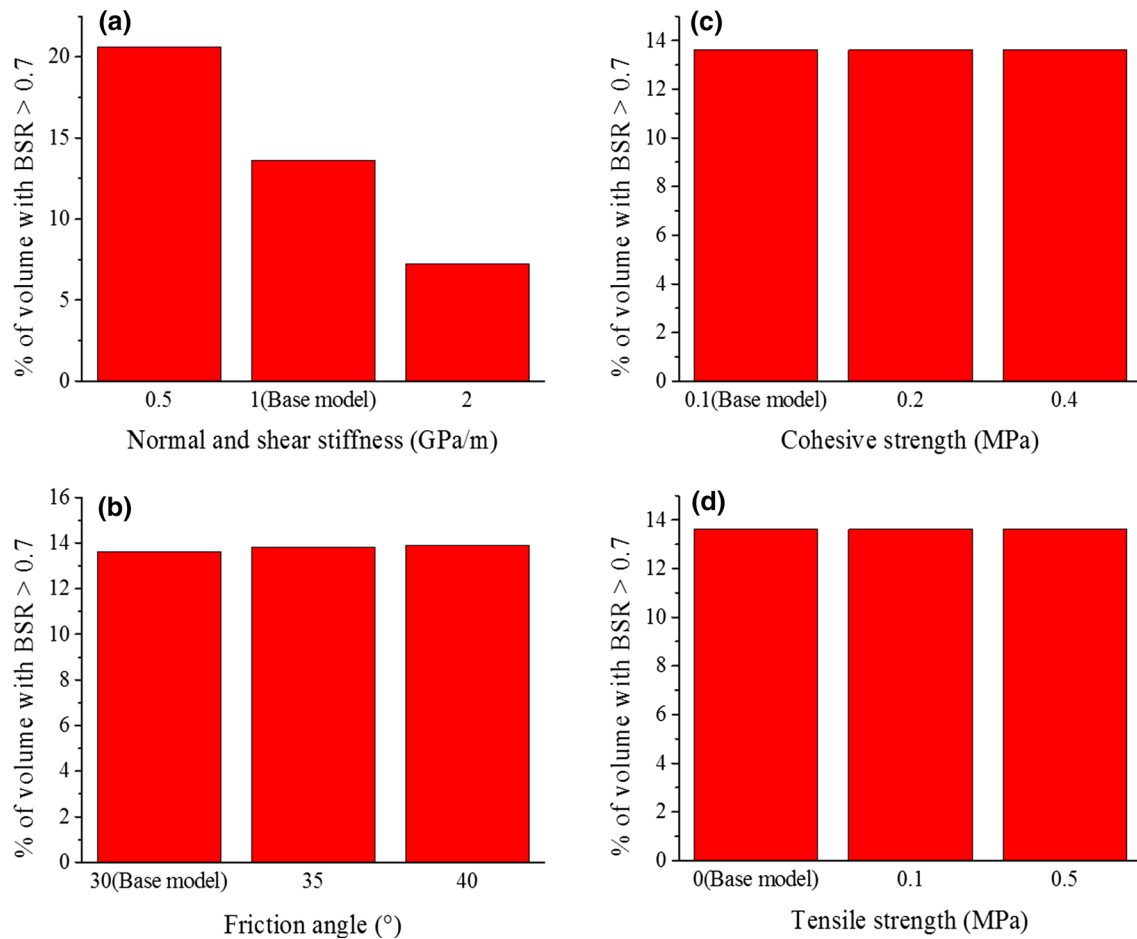


Fig. 18 Effect of mechanical properties of fractures on the stress state in the model

Table 6 Effect of fracture properties on rockburst potential

Property	Effect	Relation with BSR
Density	Major	Proportional
Length	Major	Inverse
κ in Fisher function	Minor	Inverse
Orientation	Moderate	Depends on in situ stress state
Stiffness	Major	Inverse

with the previously established indices, such as BSR and burst-prone index (Mitri et al. 1999).

4.2 Case Study Using Actual Joint Data Obtained from the Copper Cliff Mine

4.2.1 Construction of a Numerical Model with Actual Joint Sets

The joint sets shown in Table 1 are generated in a cube-shaped model in the same way as the model in Fig. 11, but in this case, the edge length of the model is set to 1.0 m.

This is due to the narrow joint spacing. The joint spacing is much smaller than that for the base model, thus requiring much denser meshes in order to minimize the effect of mesh sizes on the analysis result. Considering the difference in joint spacing between the observed joint sets and those in the base model, an appropriate average edge length of tetrahedral zones in the cube-shaped model for this case study is estimated to be 2 cm. In order to save computation time, the edge length of the cube-shaped model is set to 1 m.

The constructed model is shown in Fig. 19. It is to be noted that joints are generated in the model after performing coordinate transformation with respect to the joint orientations in Table 1. This is because the major, intermediate, and minor principal stresses at the seismic source location are applied perpendicularly to the model boundaries as shown in Fig. 13.

The numerical model shown in Fig. 19 contains all the joint sets shown in Table 1, although not all the joint sets were observed at the same location on 3710 Level. It means that the model assumes the worst case scenario with the highest, possible fracture density. It is reasonable to

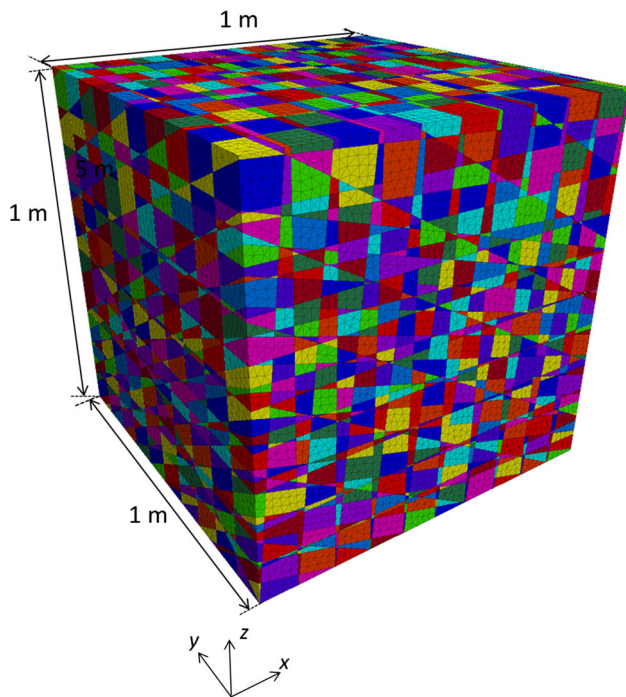


Fig. 19 Discrete element model with joint sets observed on the surface of exposed dyke on 3710 Level

assume that there are localized, highly stressed regions due to fractures and/or joint sets with high density in the dyke and that seismic events take place at such regions, triggered by mining-induced stress change.

4.2.2 Results and Discussion

The results are shown in Figs. 20 and 21. In the same fashion as the base model for the model parametrical study, complex stress fields are induced due to the generated discontinuities. In this case, approximately 5 % of the total volume (1 m^3) is changed to being significantly burst-prone. It is found from the comparison of Fig. 15 with Fig. 21 that the percentage of volume of zones with $\text{BSR} > 0.7$ for this case study is lower than that of the base model. This is conceivably attributed to the homogeneity of joints generated for this case study. As sufficient data to determine the dispersion of joint properties was not obtained from the field observation, the joint sets in Fig. 19 are deterministically generated. Consequently, discontinuities belonging to the same joint set have exactly the same spacing, which decreases the number of intersections and attenuates interactions among the joints. Nevertheless, the results explicitly show that the fracture network significantly affects the in situ stress state and contributes to the generation of burst-prone conditions. Hence, it can be concluded that there had been highly stressed regions due to preexisting discontinuities around the source location.

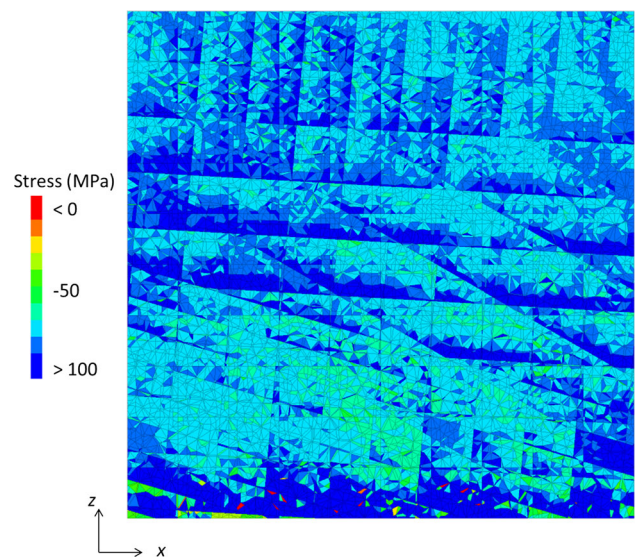


Fig. 20 Maximum compressive stress in the model for the case study

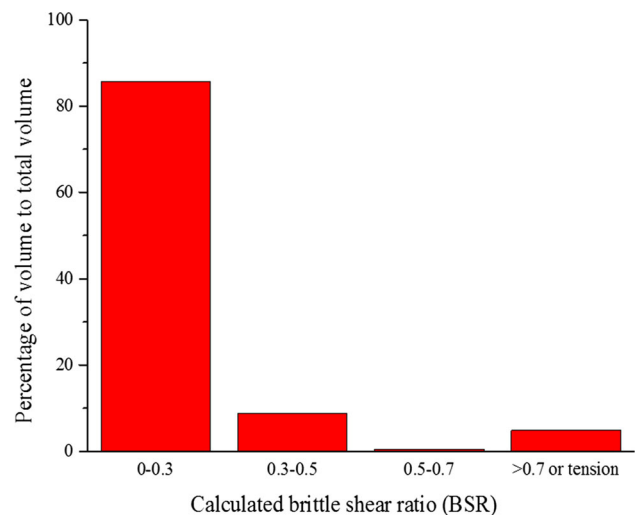


Fig. 21 Brittle shear ratio calculated for zones in the model for the case study

And then, the seismic event was triggered by the stress change due to the mining activities as demonstrated in Figs. 8 and 9. This is a plausible explanation of seismic events that take place away from active mining areas.

4.2.3 Discussion on Advantages of the Discontinuum Approach Over the Conventional Continuum Approach

It is important to discuss the advantages of the employed discontinuum analysis over the conventional continuum numerical modelling approach. First, a complex fracture network can be modelled with the discontinuum approach, which is a major advantage of this technique. It is thus

possible to replicate more representative geological conditions. In addition to that, the complicated mechanical interaction of discontinuities and resultant stress concentrations can be analyzed as demonstrated in the previous sections. It should be noted that the conventional continuum approach is also capable of taking into account stress concentrations resulting from stiffness heterogeneity within a rockmass. Stiffness heterogeneity realized in a continuum model results in low stress states within zones with low stiffness, while stress concentrates in relatively stiff zones. However, it is an implicit method which fails to accurately simulate the behavior of discontinuities and their interaction. Moreover, the continuum analysis does not allow for assigning shear and normal stiffness independently. Generally, the shear stiffness of a fracture is independent of its normal stiffness (Bandis et al. 1983). When the number of discontinuities is very small, the continuum model would yield similar results to those obtained the discontinuum model, whereas the discrepancy between the two models would become large as the number increases and the fracture network becomes more complex. As the present study focuses on a fracture network with a number of discontinuities, the discontinuum model is more appropriate.

5 Conclusion

A case study of a large seismic event that took place on 3880 Level at the Copper Cliff mine, Sudbury, Canada, is undertaken. A stress analysis of a 3D orebody-wide model indicates that the stress state at the seismic event source location is not high enough for such a seismic event to occur when the geological structures such as the dyke are treated as homogenous. In light of this result, it is postulated that there had been highly stressed regions caused by preexisting fractures and/or joints around the source location before the seismic event took place. In order to verify the postulation, a cube-shaped model is constructed, and a fracture network is generated in the model by means of the discrete modelling technique. The results obtained from a model parametrical study show that the fracture network significantly affects the stress state and generates burst-prone conditions. It is found that the fracture density, length, and stiffness have a large influence on the stress state, while the friction angle, cohesion, and tensile strength of the fractures have lesser influences under the in situ stress state. When the fracture length is short, almost 50 % of the total volume becomes extremely high burst-prone conditions. Finally, a cube-shaped discrete model with joint sets actually observed at the mine is constructed, and a stress analysis is performed. As is the case with the model parametrical study, it is demonstrated

that the generated fracture network causes complex stress fields with high stress concentrations in the model. Hence, through the stress analyses with the discrete modelling technique, the postulation is numerically verified. It is not uncommon that large seismic events take place within geologically disturbed regions away from active mining areas. The present study numerically demonstrates the contribution of fracture network to the generation of burst-prone stress state leading to significant seismic events. It is thus suggested that a new index taking into consideration the effect of fracture network properties on in situ stress fields be established as future work in order to assess rockburst potential in geologically disturbed regions.

Acknowledgments This work is financially supported by a grant by the Natural Science and Engineering Research Council of Canada (NSERC) in partnership with Vale Canada Ltd—Ontario Operations under the Collaborative Research and Development Program. The authors are grateful for their support.

References

- Alber M, Fritschen R (2011) Rock mechanical analysis of a $M1 = 4.0$ seismic event induced by mining in the Saar District, Germany. *Geophys J Int* 186:359–372
- Bandis S, Lumsden AC, Barton NR (1983) Fundamentals of rock joint deformation. *Int J Rock Mech Min Sci Geomech* 20(6):249–268
- Barton N (1973) Review of a new shear-strength criterion for rock joints. *Eng Geol* 7:287–332
- Barton N (2013) Shear strength criteria for rock, rock joints, rockfill and rock masses: problems and some solutions. *J Rock Mech Geotech Eng* 5:249–261
- Barton N, Choubey V (1977) The shear strength of rock joints in theory and practice. *Rock Mech* 10:1–54
- Bewick RP, Valley B, Runnals S, Whitney J, Krynicki Y (2009) Global approach to managing deep mining hazard. In: *The 3rd CANUS rock mechanics symposium*, Toronto
- Bieniawski ZT (1976) Rock mass classification in rock engineering. In: *Exploration for rock engineering*. Balkema, Cape Town
- Blake W, Hedley DGF (2003) Rockbursts case studies from North America Hard-Rock Mines. In: *Society for mining, metallurgy, and exploration*, Littleton, Colorado, USA
- Castro LM, Bewick RP, Carter TG (2012) An overview of numerical modelling applied to deep mining. CRC Press/Taylor & Francis, London, pp 393–414
- Diederichs MS (1999) Instability of hard rockmass: the role of tensile damage and relaxation. University of Waterloo, Waterloo
- Diederichs MS, Kaiser PK, Eberhardt E (2004) Damage initiation and propagation in hard rock during tunnelling and the influence of near-face stress rotation. *Int J Rock Mech Min Sci* 41:785–812
- Fisher NI (1996) Statistical analysis of circular data. Cambridge University Press, Cambridge
- Hedley DGF (1992) Rockburst handbook for Ontario hard rock mines. Ontario Mining Association, North York
- Hergert G (1987) Stress assumptions for underground excavations in the Canadian Shield. *Int J Rock Mech Min Sci Geomech Abstr* 24(1):95–97
- Heunis R (1980) The development of rock-burst control strategies for South African gold mines. *S Afr Inst Min Metall* 80(4):139–150

- Hoek E, Bieniawski ZT (1965) Brittle fracture propagation in rock under compression. *Int J Fract Mech* 1(3):137–155
- Hoek E, Brown ET (1997) Practical estimates of rock mass strength. *Int J Rock Mech Min Sci* 34(8):1165–1186
- Hoek E, Martin CD (2014) Fracture initiation and propagation in intact rock—a review. *J Rock Mech Geotech Eng* 6:287–300
- Hooker JN, Laubach SE, Marrett R (2014) A universal power-law scaling exponent for fracture apertures in sandstones. *Geol Soc Am Bull* 127(3–4):516–538
- Itasca (2009) *FLAC3D—fast Lagrangian analysis of continua*. Itasca Consulting Group Inc., USA
- Itasca (2014) *3DEC—3 dimensional distinct element code, version 5.0*. ICG, Minneapolis
- Kidybinski A (1981) Bursting liability indices of coal. *J Rock Mech Min Sci* 18(4):295–304
- Ledwada LS, Scheepers J, Durrheim RJ (2012) Rockburst damage mechanism at Impala platinum. In: Southern hemisphere international rock mechanics symposium SHIRMS 2012, pp 367–386
- Martin CD, Kaiser PK (1999) Predicting the depth of stress induced failure around underground excavations in brittle rocks. In: 49th Canadian geotechnical conference St. John's, Newfoundland, pp 105–114
- McGarr A, Spottiswoode SM, Gay NC (1975) Relationship of mine tremors to induced stresses and to rock properties in the focal region. *Bull Seismol Soc Am* 65(4):981–993
- Mitri HS, Edrissi R, Henning J (1994) Finite element modelling of cable-bolted slopes in hardrock ground mines. In: SME Annual Meeting, Albuquerque, New Mexico, pp 94–116
- Mitri HS, Tang B, Simon R (1999) FE modelling of mining-induced energy release and storage rates. *J S Afr Inst Min Metall* 99(2):103–110
- Ortega OJ, Marrett RA, Laubach SE (2010) A scale-independent approach to fracture intensity and average spacing measurement. *Am Assoc Petrol Geol* 90(2):193–208
- Ortlepp WD, Stacey TR (1994) Rockburst mechanisms in tunnels and shafts. *Tunn Undergr Space Technol* 9:59–65
- Pola A, Crosta GB, Fusi N, Castellanza R (2014) General characterization of the mechanical behaviour of different volcanic rocks with respect to alteratino. *Eng Geol* 169:1–13
- Qiu S, Feng X, Zhang C, Xiang T (2014) Estimation of rockburst wall-rock velocity invoked by slab flexure sources in deep tunnels. *Can Geotech J* 51:520–539
- Sainoki A, Mitri HS (2014) Methodology for the interpretation of fault-slip seismicity in a weak shear zone. *J Appl Geophys* 110:126–134. doi:10.1016/j.jappgeo.2014.09.007
- Shnorhokian S, Mitri HS, Thibodeau D (2014) Numerical simulation of pre-mining stress field in a heterogeneous rockmass. *Int J Rock Mech Min Sci* 66:13–18
- Wawersik WK, Fairhurst CA (1970) A study of brittle rock fracture in laboratory compression experiments. *Int J Rock Mech Min Sci Geomech* 7:561–575